Deposition of Pr- and Nd-aluminate by Liquid Injection MOCVD and ALD Using Single-Source Heterometallic Alkoxide Precursors

Jeffrey M. Gaskell,[†] Szymon Przybylak,[†] Anthony C. Jones,*[,†,‡] Helen C. Aspinall,*[,†] Paul R. Chalker,[§] Kate Black,[§] Richard J. Potter,[§] Pouvanart Taechakumput,[||] and Stephen Taylor[||]

Department of Chemistry, University of Liverpool, Liverpool L69 7ZD, United Kindgom, Department of Engineering, University of Liverpool, Liverpool L69 3BX, United Kingdom, Department of Electrical Engineering and Electronics, University of Liverpool, Liverpool L69 3GJ, United Kingdom, and Epichem Limited, Power Road, Bromborough, Wirral, Merseyside CH62 3QF, United Kingdom

Received March 19, 2007. Revised Manuscript Received May 17, 2007

Thin films of praseodymium aluminate ($PrAlO_x$) and neodymium aluminate ($NdAlO_x$) have been deposited by liquid injection metalorganic chemical vapor deposition (MOCVD) and atomic layer deposition (ALD) using the bimetallic alkoxide precursors $[PrAl(OPr^i)_6(Pr^iOH)]_2$ and $[NdAl(OPr^i)_6(Pr^iOH)]_2$. Auger electron spectroscopy showed that all the films were high purity, with no carbon detectable (est. detection limit ≈ 0.5 at %). X-ray diffraction showed that the $PrAlO_x$ and $NdAlO_x$ films remained amorphous up to temperatures of 900 °C. Films grown by ALD were all Pr- or Nd-deficient (Pr/Al = 0.54−0.71; Nd/Al = 0.30−0.42), but near-stoichiometric films of $PrAlO_x$ (Pr/Al = 0.76) and $NdAlO_x$ (Nd/Al = 0.87) were obtained by MOCVD at deposition temperatures of 500 and 450 °C, respectively. The electrical properties of the films were assessed using $C-V$ and $I-V$ on MOS capacitors. Post-metalization annealing (PMA) in forming gas was effective in reducing charge levels in all films. Following PMA, the dielectric properties of $NdAlO_x$ were superior to those of $PrAlO_x$, MOSCs fabricated with $NdAl_xO_y$ (Nd/Al = 0.87) and $PrAlO_x$ (Pr/Al = 0.76) showed leakage current densities below 7.5×10^{-10} A cm^{-2} ($\kappa \sim 14$) and 1×10^{-6} A cm^{-2} ($\kappa \approx 12$), respectively.

Introduction

The rapid shrinking, or scaling, in the dimensions of the field effect transistor (FET) in complementary metal-oxide semiconductor (CMOS) technology has also forced the channel length and gate dielectric thickness to decrease rapidly.[1] As the dimensions of the SiO_2 layer approach 2−3 nm, direct electron tunneling and high leakage currents present serious obstacles to future device reliability.[2] The use of materials with a higher dielectric constant than SiO_2 ($\kappa = 3.9$) allows an equivalent capacitance to be achieved in a physically thicker insulating layer, which should provide reduced leakage currents. There has thus been much recent research aimed at replacing the conventional SiO_2 gate dielectric material with alternative high-κ dielectric oxides or silicates.[2,3] There has also been a corresponding effort to utilize high-κ oxides as capacitor layers in next-generation DRAM technologies.[4]

Although ZrO_2, HfO_2 and their associated silicates and aluminates have been the most intensively investigated high-κ materials,[2] there has been much recent interest in the lanthanide oxides.[5] The oxides M_2O_3 (M = La, Pr, Gd, Nd) are good insulators because of their large band gaps (3.9 eV for Pr_2O_3, 5.6 eV for Gd_2O_3). They also have high dielectric constants (Nd_2O_3 $\kappa = 12.64$, La_2O_3 $\kappa = 30$, Pr_2O_3 $\kappa = 26-30$), high symmetrical band offsets relative to Si (>1 eV for Pr_2O_3) and good thermodynamic stability on silicon, making them attractive candidates for high-κ CMOS and DRAM applications.

However, the binary lanthanide oxides suffer from various drawbacks in their material properties, which have hindered their application in microelectronics. For instance, La_2O_3 is chemically unstable, readily converting to $La_2(CO_3)_3$ during growth or upon storage or annealing,[6,7] and is easily converted to $La(OH)_3$ on reaction with ambient water.[7,8] They also undergo an amorphous to polycrystalline transition at moderate temperatures (ca. 400−450 °C for Gd_2O_3[9] and Nd_2O_3[10]). This can lead to a large increase in leakage current

* Corresponding author. E-mail: hca@liv.ac.uk (H.C.A.).
[†] Department of Chemistry, University of Liverpool.
[‡] Epichem Limited.
[§] Department of Engineering, University of Liverpool.
[||] Department of Electrical Engineering and Electronics, University of Liverpool.

(1) Packan, P. A. *Science* **1999**, *285*, 2079.
(2) Wilk, G. D.; Wallace, R. M.; Anthony, J. M. *J. Appl. Phys.* **2001**, *89*, 5243.
(3) (a) Jones, A. C. *Chem. Vap. Deposition* **2006**, *12*, 81. (b) Päiväsaari, J.; Niinistö, J.; Myllymäki, P.; Dezelah, C.; Winter, C. H.; Putkonen, M.; Nieminen, M.; Niinistö, L. *Top. Appl. Phys.* **2007**, *106*, 15−32.
(4) Zhu, C. X.; Cho, B. J.; Li, M. F. *Chem. Vap. Deposition* **2006**, *12*, 165.
(5) Leskela, M.; Ritala, M. *J. Solid State Chem.* **2003**, *171*, 170.
(6) Gougousi, T.; Niu, D.; Ashcraft, R. W.; Parsons, G. N. *Appl. Phys. Lett.* **2003**, *83*, 3543.
(7) Nieminen, M.; Putkonen, M.; Niinisto, L. *Appl. Surf. Sci.* **2001**, *174*, 155−165.
(8) Cheng, J. B.; Li, A. D.; Shao, Q. Y.; Ling, H. Q.; Wu, D.; Wang, Y.; Bao, Y. J.; Wang, M.; Liu, Z. G.; Ming, N. B. *Appl. Surf. Sci.* **2004**, *233*, 91.
(9) Aspinall, H. C.; Gaskell, J. M.; Loo, Y. F.; Jones, A. C.; Chalker, P. R.; Potter, R. J.; Smith, L. M.; Critchlow, G. W. *Chem. Vap. Deposition* **2004**, *10*, 301.

10.1021/cm0707556 CCC: $37.00
Published on Web 08/16/2007

and the growth of a low-κ SiO_2 interfacial layer during CMOS processing, which involves a high-temperature (>800 °C) annealing step.

The lanthanide aluminates, $MAlO_3$ (M = La, Pr, Gd, Nd, etc.), are promising high-κ materials, as they combine the advantages of the high permittivity of the lanthanide oxide-with the chemical and thermal stability of Al_2O_3. Furthermore, they remain amorphous up to high temperatures (eg. $LaAlO_x$ remains amorphous up to 850 °C[11]), leading to a large reduction in leakage current relative to polycrystalline M_2O_3 films and to inhibition of the growth of a SiO_2 interfacial layer during CMOS processing.

There are very few reports on the deposition of $NdAlO_x$ and $PrAlO_x$ by either PVD or CVD techniques. $NdAlO_x$ thin films have been deposited by pulsed laser deposition,[12] e-beam evaporation,[13] sol−gel deposition,[14] and ALD,[15] whereas nanometer-sized $NdAlO_x$ crystals have been grown in an amorphous Al_2O_3 matrix by MOCVD using the heterometal alkoxide $[Nd\{Al(OPr^i)_4\}_3(Pr^iOH)]$.[16] The analogous Pr/Al heterometal alkoxide has also been used in MOCVD to deposit $PrAlO_x$ nanocrystals in an Al_2O_3 matrix,[16] and the ALD of $PrAlO_x$ has recently been reported.[17]

The ALD of $NdAlO_x$ was achieved using $[Nd(thd)_3]$ (thd = 2,2,6,6-tetramethylheptane-3,5-dionato), $[AlMe_3]$, and ozone or H_2O.[15] The $NdAlO_x$ films deposited at 300 °C were amorphous, but crystallized during annealing in nitrogen or oxygen at 850−900 °C. $[Pr(amd)_3]$ (amd = *N*,*N*′-diisopropylacetamidinato), $[AlMe_3]$, and H_2O have been used for the ALD of $PrAlO_x$.[17] A film with the stoichiometry $Pr_{1.15}Al_{0.85}O_3$ had a permittivity of 18, and all annealed films demonstrated low leakage currents ($\sim 1.1 \times 10^{-4}$ A cm^{-2}).

The use of these precursors in ALD requires careful control of the alternating La, Al, and H_2O precursor pulses to deposit the $LaAlO_x$ films, and the hazardous pyrophoric precursor $[AlMe_3]$ is required as the Al source. A simpler approach is to utilize "single-source" precursors containing the lanthanide and Al atoms in the required 1:1 stoichiometry.

"Single-source" precursors have seldom been used for the ALD of multicomponent oxides, although the ALD of $SrTa_2O_6$ by ALD using $[Sr\{Ta(OEt)_5(dmae)\}_2]$ (dmae = 2-dimethylaminoethanolate) has been demonstrated.[18] We have recently reported the liquid injection ALD[11] and MOCVD[11,19] of $LaAlO_x$ using $[LaAl(OPr^i)_6(Pr^iOH)]_2$. The stoichiometry of the MOCVD-grown films showed a marked dependence on growth temperature, becoming La deficient at high growth temperatures,[11,19] probably because of thermal decomposition of the precursor. The ALD-grown $LaAlO_x$ films were all La-deficient with La/Al ratios varying from 0.50 to 0.61.[11] An ALD-grown film with a La/Al ratio of 0.54 showed good dielectric properties (*C*−*V*) with a low shift in the flatband voltage (V_{FB}) and a permittivity κ of ~13. An ALD-grown $LaAlO_x$ film (La/Al = 0.54) had a leakage current density of 7×10^{-8} A cm^{-2}, whereas an MOCVD-grown film (La/Al = 2.5) had a leakage current density of 2×10^{-7} A cm^{-2}.[11]

We now report an extension of these studies, and we describe the use of $[LnAl(OPr^i)_6(Pr^iOH)]_2$ (Ln = Pr, Nd) for the growth of $PrAlO_x$ and $NdAlO_x$ by liquid injection ALD and MOCVD.

Experimental Section

All manipulations were carried out under an atmosphere of dry nitrogen using standard Schlenk line or dry box techniques. Anhydrous $NdCl_3$ and $PrCl_3$ were prepared by dehydration of the hydrated chlorides in the presence of NH_4Cl followed by removal of NH_4Cl by sublimation. $[Al(OPr^i)_3]$ was obtained from Aldrich Chemical Co.

Auger electron spectroscopy (AES) was carried out on a Varian scanning Auger spectrometer. The atomic compositions quoted are from the bulk of the film (typically 70−80 nm depth), free from surface contamination, and were obtained by combining AES with sequential argon ion bombardment until comparable compositions were obtained for consecutive data points. Compositions were based on Ln_2O_3 (Ln = Pr, Nd) and Al_2O_3 powder reference materials.

Thermogravimetric analysis (TGA) was carried out on a Shimadzu TG-51A thermogravimetric analyzer using a heating rate of 10 °C/min. The masses of $[LnAl(OPr^i)_6(Pr^iOH)]_2$ samples used in the TGA were 41.7 mg (Ln = Nd) and 33.8 mg (Ln = Pr) The carrier gas was nitrogen and the TGA apparatus was housed in a N_2-filled glove box, so that the analysis was carried out under fully anaerobic conditions.

Precursor Synthesis. The $[LnAl(OPr^i)_6(Pr^iOH)]_2$ (Ln = Pr, Nd) complexes were synthesized in an analogous manner to that described for $[LaAl(OPr^i)_6(Pr^iOH)]_2$.[11]

$[PrAl(OPr^i)_6(Pr^iOH)]_2$. Anhydrous $PrCl_3$ (7.822 g, 0.032 mol) was sonicated for 1 h with dry propan-2-ol (40 cm^3) in toluene (200 cm^3). To the $PrCl_3 \cdot 3Pr^iOH$ suspension was added $Al(Pr^iO)_3$ (6.461 g, 0.032 mol) and K metal (3.710, 0.095 mol) at −50 °C. The mixture was then refluxed for 48 h. The solution was separated from the precipitated KCl by filtration and volatiles were removed in vacuo. The crude product was recrystallized from a pentane to give a pale green crystals (9.110 g, 49.4%). Elemental anal. Calcd for $C_{42}H_{100}Al_2O_{14}Pr_2$: C, 43.30; H, 8.65; Al, 4.63; Pr, 24.19. Found: C, 42.85; H, 8.32; Al, 4.80; Pr, 23.99.

$[NdAl(OPr^i)_6(Pr^iOH)]_2$. $[NdAl(OPr^i)_6(Pr^iOH)]_2$ was synthesized as above from anhydrous $NdCl_3$ (9.178 g, 0.037 mol), $Al(Pr^iO)_3$ (7.481 g, 0.037 mol), and K metal (4.296, 0.110 mol). The crude product was recrystallized from a pentane to give pale lilac crystals (10.677 g, 49.8%). Elemental anal. Calcd for $C_{42}H_{100}Al_2O_{14}Nd_2$: C, 43.05; H, 8.60; Al, 4.61; Nd, 24.62. Found: C, 42.82; H, 7.90; Al, 4.68; Nd, 25.01.

(10) Loo, Y. F.; Potter, R. L.; Jones, A. C.; Aspinall, H. C.; Gaskell, J. M.; Chalker, P. R.; Smith, L. M.; Critchlow, G. W. *Chem. Vap. Deposition* **2004**, *10*, 306.
(11) Gaskell, J. M.; Jones, A. C.; Aspinall, H. C.; Przybylak, S.; Chalker, P. R.; Black, K.; Davies, H. O.; Taechakumput, P.; Taylor, S.; Critchlow, G. W. *J. Mater. Chem.* **2006**, *16*, 3854.
(12) Rao, M. R. *Thin Solid Films* **1997**, *306*, 141.
(13) Brugnoni, C.; Ducati, U.; Chemelli, C.; Scagliotti, M.; Chiodelli, G. *Solid State Ionics* **1995**, *76*, 183.
(14) Mathur, S.; Veith, M.; Shen, H.; Lecerf, N.; Hufner, S. *Scr. Mater.* **2001**, *44*, 2105.
(15) Kosola, A.; Päiväsaari, J.; Putkonen, M.; Niinistö, L.. *Thin Solid Films* **2005**, *479*, 152.
(16) Veith, M.; Mathur, S.; Shen, H.; Lecerf, N.; Hufner, S.; Jilavi, M. H. *Chem. Mater.* **2001**, *13*, 4041.
(17) de Rouffignac, P.; Gordon, R. G. *Chem. Vap. Deposition* **2006**, *12*, 152.
(18) Vehkamaki, M.; Ritala, M.; Leskela, M.; Jones, A. C.; Davies, H. O.; Sajavaara, T.; Rauhala, E. *J. Electrochem. Soc.* **2004**, *151*, F69.
(19) Manning, T. D.; Loo, Y. F.; Jones, A. C.; Aspinall, H. C.; Chalker, P. R.; Bickley, J. F.; Smith, L. M.; Critchlow, G. W. *J. Mater. Chem.* **2005**, *15*, 3384.

Table 1. Growth Conditions Used for the Deposition of $PrAlO_x$ and $NdAlO_x$ by Liquid Injection MOCVD using $[LnAl(OPr^i)_6(Pr^iOH)]_2$ (Ln = Pr or Nd)

	$PrAlO_x$	$NdAlO_x$
substrate temperature (°C)	250−600 (Si 100)	300−600 (Si 100)
evaporator temperature (°C)	200	200
pressure (mbar)	5	5
injection rate ($cm^3\,h^{-1}$)	30	30
solvent	toluene	toluene
concentration (M)	0.05	0.05
argon flow ($cm^3\,min^{-1}$)	200	200
oxygen flow ($cm^3\,min^{-1}$)	100	100
run time (min)	10	10

Table 2. Growth Conditions Used for the Deposition of $PrAlO_x$ and $NdAlO_x$ by Liquid Injection ALD using $[LnAl(OPr^i)_6(Pr^iOH)]_2$ (Ln = Pr or Nd)

	$PrAlO_x$	$NdAlO_x$
substrate temperature (°C)	180−350	180−350
evaporator temperature (°C)	175	175
pressure (mbar)	5	5
injection rate (μL/pulse)	2.5 (4 pulses/cycle)	2.5 (4 pulses/cycle)
solvent	toluene	toluene
concentration (M)	0.05	0.05
argon flow ($cm^3\,min^{-1}$)	200	200
pulse sequence (precursor/purge/water/purge)	2/2/0.5/3.5	2/2/0.5/3.5
no. of cycles	400	400

MOCVD and ALD. Liquid injection MOCVD and ALD experiments were carried out on an Aixtron AIX 200FE AVD reactor fitted with the "Trijet" liquid injector system.[20] During the MOCVD experiments, oxygen was introduced at the inlet of the reactor. For the ALD experiments, the oxidant was replace by water vapor, which was controlled by a pneumatic valve. The substrate was rotated throughout all experiments. Films of praseodymium aluminate and neodymium aluminate were deposited on Si (100) substrates using a 0.05 M solution of either $[PrAl(O^iPr)_6(Pr^iOH)]_2$ or $[NdAl(O^iPr)_6(Pr^iOH)]_2$ in toluene. Full MOCVD and ALD growth conditions can be found in Tables 1 and 2 .

Growth rates were calculated from the weight gained by the substrate during the growth run. Film thicknesses were calculated by assuming the film has the same density as $LaAlO_3$ (6.57 g cm^{-3}).

Electrical Assessment. To assess electronic properties of the gate dielectric, we fabricated MOS capacitors (MOSCs) by thermal evaporation of aluminum gates through a shadow mask with an effective area of 4.9×10^{-4} cm^2. High-frequency capacitance-voltage (HFCV) measurements were conducted using a HP4192 impedance analyzer with a 30 mV rms probe signal. Measurements were performed in parallel mode from a strong inversion toward a strong accumulation (vice versa), with a sweep rate of 0.01 V/s, at various frequencies (1 kHz to 1 MHz). The measured capacitance was also corrected for series resistance effect and leaky oxides following the methodology presented elsewhere.[21] Current−voltage measurements ($I-V$) were performed using a Keithley K230 programmable voltage source and 617 type electrometer. The films were then subsequently post-metalization annealed (PMA) in forming gas (10% hydrogen and 90% nitrogen mixture gases) at 380 °C for 15 min, and the effect of PMA on electronic properties was investigated.

Results and Discussion

For successful use in MOCVD and ALD, it is important that the precursor evaporates cleanly, without decomposition at moderate temperatures. Thermogravimetric analysis (TGA) data for $[PrAl(OPr^i)_6(Pr^iOH)]_2$ and $[NdAl(OPr^i)_6(Pr^iOH)]_2$ are shown Figure 1. The data show that $[PrAl(OPr^i)_6(Pr^iOH)]_2$ evaporates in the temperature range 200−380 °C and that $[NdAl(OPr^i)_6(Pr^iOH)]_2$ is slightly more volatile, evaporating at 180−350 °C. Both complexes leave relatively little residue (~2.5%). Shoulders in the TGA curve at 200−250 (Pr) and 180−220 °C (Nd) can be attributed to loss of the weakly coordinating Pr^iOH ligand from the complexes. (Theoretical weight loss for loss of Pr^iOH from $[NdAl(OPr^i)_6(Pr^iOH)]_2$ = 10.26% and from $[PrAl(OPr^i)_6(Pr^iOH)]_2$ = 10.32%.)

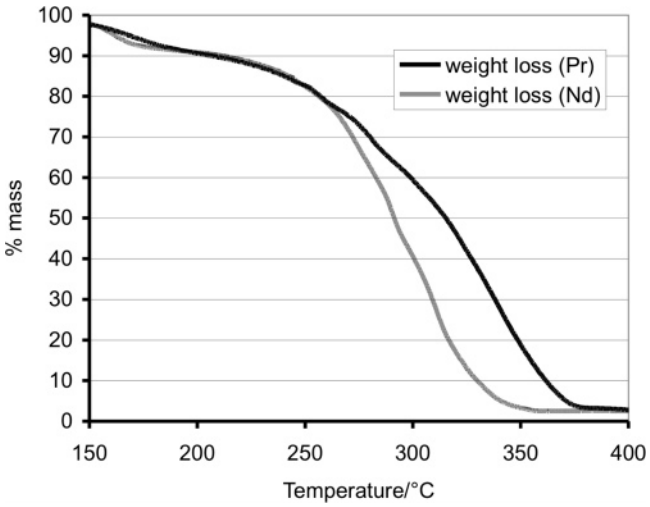

Figure 1. Thermogravimetric analysis of $[PrAl(OPr^i)_6(Pr^iOH)]_2$ and $[[NdAl(OPr^1)_6(Pr^1OH)]_2$.

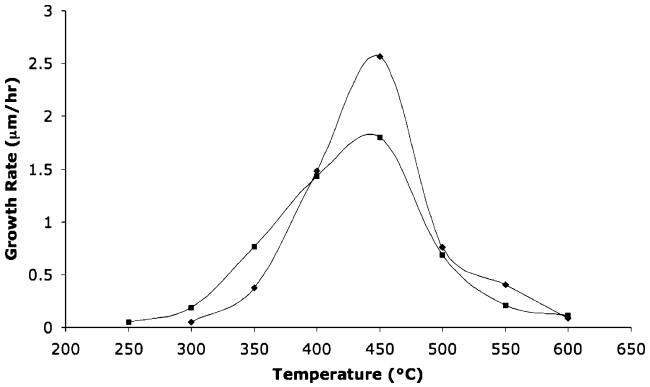

Figure 2. Variation of growth rate with substrate temperature for $LnAlO_x$ films grown by liquid injection MOCVD using $[NdAl(OPr^i)_6(Pr^iOH)]_2$ (◆) and $[PrAl(OPr^i)_6(Pr^iOH)]_2$ (■).

Figure 2 shows the effect of growth temperature on the growth rate for both $PrAlO_x$ and $NdAlO_x$ by liquid injection MOCVD.

The growth rate of $PrAlO_x$ by MOCVD increases in the temperature range of 250−450 °C. This corresponds to the region of kinetic control in which the film growth is dominated by thermal decomposition of the precursor onto the substrate. The oxide growth rate reaches a maximum at 450 °C before decreasing rapidly because of thermal depletion of the precursor in the gas phase and on the reactor.

The growth curve of $NdAlO_x$ by MOCVD is very similar to that of $PrAlO_x$, showing a region of kinetic control

(20) Potter, R. J.; Chalker, P. R.; Manning, T. D.; Aspinall, H. C.; Loo, Y. F.; Jones, A. C.; Smith, L. M.; Critchlow, G. W.; Schumacher, M. *Chem. Vap. Deposition* **2005**, *11*, 159.

(21) Kwa, K. S. K.; Chattopadhyay, S.; Jankovic, N. D.; Olsen, S. H.; Driscoll, L. S.; O'Neill, A. G. *Semicond. Sci. Technol.* **2003**, *18*, 82.

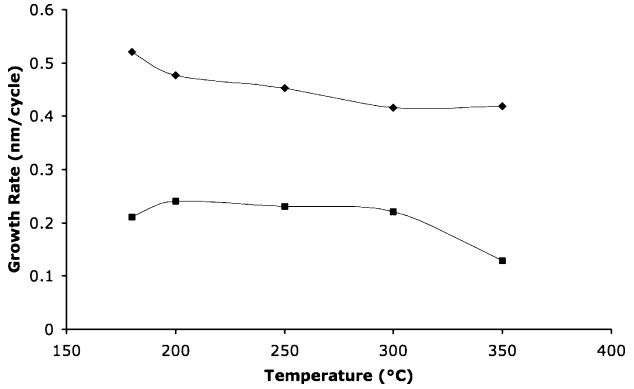

Figure 3. Variation of growth rate with substrate temperature for $LnAlO_x$ films grown by liquid injection ALD using $[NdAl(OPr^i)_6(Pr^iOH)]_2$ (◆) and $[PrAl(OPr^i)_6(Pr^iOH)]_2$ (■).

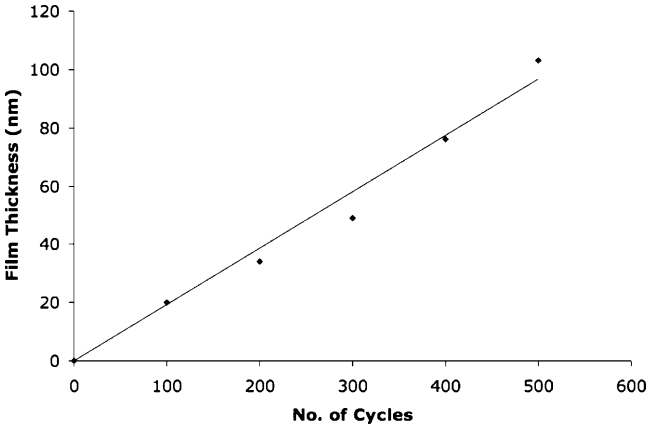

Figure 4. Variation of film thickness with number of ALD cycles for $PrAlO_x$ films grown by liquid injection ALD using $[PrAl(OPr^i)_6(Pr^iOH)]_2$.

between 300 and 450 °C, a maximum at 450 °C, and a decrease in growth rate due to thermal depletion in the gas phase between 450 and 600 °C. The maximum growth rate of $NdAlO_x$ is approximately 60% greater than that of $PrAlO_x$ (2.56 μm/h compared to 1.8 μm/h), consistent with the higher volatility of the $[NdAl(OPr^i)_6(Pr^iOH)]_2$ precursor as indicated by TGA. In turn, the maximum growth rates of these two materials are greater than of the previously reported MOCVD of $LaAlO_x$ at 450 °C from the analogous precursor $[LaAl(O^iPr)_6(Pr^iOH)]_2$ (0.924 μm/h).[11] The trend of increasing growth rate across the lanthanide series is most likely due to the extra volatility associated with the decreasing size of the lanthanide metal. The temperature for the onset of growth increases across the series, indicating an increase in thermal stability as the size of the lanthanide decreases.

Figure 3 shows the effect of growth temperature on the growth rate for both $PrAlO_x$ and $NdAlO_x$ by liquid injection ALD. The growth rates have been normalized with respect to moles of injected precursor to allow a direct comparison between the growth curves of each material.

The growth rate of $PrAlO_x$ by ALD remains relatively consistent over the temperature range 180−300 °C (~0.23 nm/cycle). The growth rate decreases at 350 °C because of desorption from the substrate surface. This indicates that the precursor is thermally stable up to 350 °C. The growth rate of $NdAlO_x$ by ALD is higher than that seen for the ALD of $PrAlO_x$ over the same temperature range, with a maximum of 0.52 nm/cycle at 180 °C. The growth rate steadily

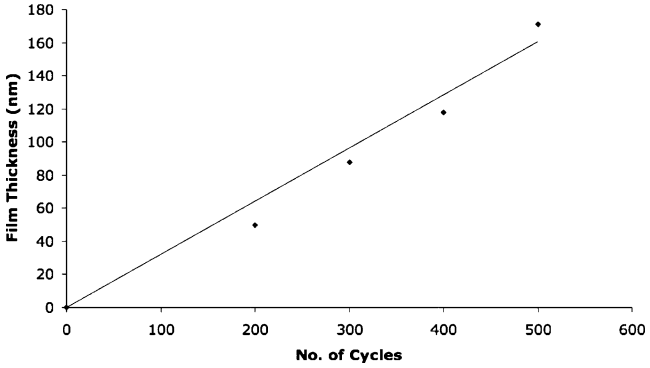

Figure 5. Variation of film thickness with number of ALD cycles for $NdAlO_x$ films grown by liquid injection ALD using $[NdAl(OPr^i)_6(Pr^iOH)]_2$.

Table 3. Auger Electron Spectroscopy Data Showing the Composition (at %) of $PrAlO_x$ Films Deposited by Liquid Injection MOCVD and ALD Using $[PrAl(OPr^i)_6(Pr^iOH)]_2$

T	technique	sample	Pr	Al	O	Pr/Al
250	MOCVD	880	21.2	12.5	66.3	1.70
300	MOCVD	875	24.6	11.1	64.4	2.22
350	MOCVD	874	23.1	13.2	63.8	1.75
450	MOCVD	877	20.3	10.4	69.3	1.95
500	MOCVD	878	22.7	29.9	47.3	0.76
180	ALD	883	15	26.8	58.2	0.56
250	ALD	884	12.3	17.3	70.4	0.71
300	ALD	885	14.5	25.2	60.4	0.58

Table 4. Auger Electron Spectroscopy Data Showing the Composition (at %) of $NdAlO_x$ Films Deposited by Liquid Injection MOCVD and ALD Using $[NdAl(OPr^i)_6(Pr^iOH)]_2$

T	technique	sample	Nd	Al	O	Nd/Al
300	MOCVD	910	16.1	14.4	69.5	1.12
350	MOCVD	909	29.3	13.5	57.2	2.17
400	MOCVD	908	25.1	18.7	56.2	1.34
450	MOCVD	911	20.1	23.2	56.7	0.87
500	MOCVD	912	16	29.5	54.5	0.54
180	ALD	916	10.3	34.5	55.3	0.30
250	ALD	917	9.9	31.8	58.3	0.31
350	ALD	919	12.9	30.7	56.4	0.42

decreases over the temperature range 180−350 °C, which can also be ascribed to desorption from the substrate surface. This shows that the precursor is thermally stable up to 350 °C. The growth of $NdAlO_x$ by ALD was not self-limiting, with the growth rate increasing with injected volume of precursor/cycle. This is consistent with the lack of self-limiting ALD previously observed for $[La(Al(OPr^i)_6(Pr^iOH)]_2$[11] and can be attributed to precursor decomposition via β-hydride elimination from the $[OPr^i]$ ligand,[11] or to the presence of trace residual water inside the modified MOCVD reactor which had not been fully removed during the purge step. No growth was seen with either precursor at 200 °C in the absence of water. The growth rate of both $PrAlO_x$ and $NdAlO_x$ had a linear relationship with the number of ALD cycles showing that the deposition of both materials was highly controllable, as shown in Figure 4 and 5 .

The atomic compositions of the $PrAlO_x$ and $NdAlO_x$ films were determined by Auger electron spectroscopy (AES) and the data are shown in Tables 3 and 4. All the films are of a high purity, with carbon not detected at an estimated detection limit of 0.5 at %. The AES data show that the $PrAlO_x$ and $NdAlO_x$ films grown by ALD are all lanthanide-deficient. The Pr/Al ratio varies from 0.56 to 0.71, whereas the Nd/Al ratio varies from 0.30 to 0.42. A similar

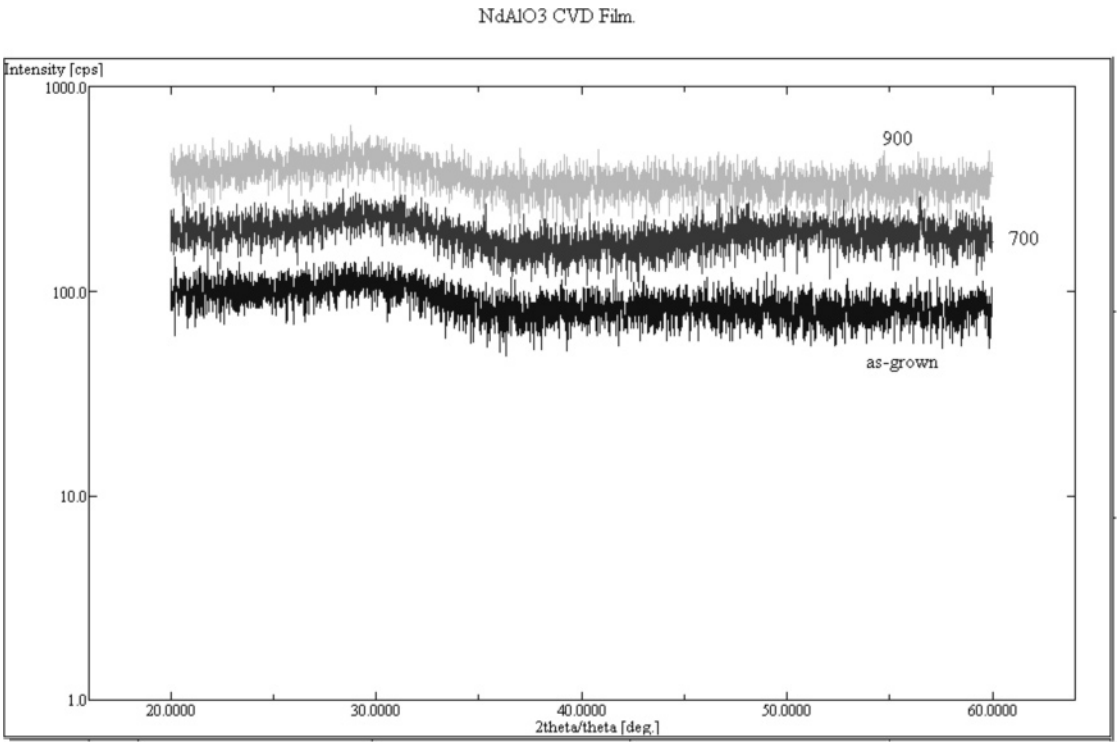

Figure 6. X-ray diffraction data for a $NdAlO_x$ film (Nd/Al = 1.34) grown by MOCVD at 400 °C and then annealed in air at 700 and 900 °C.

compositional effect was observed in $LaAlO_x$ films deposited by liquid injection ALD[11] in which La/Al ratios of 0.50 to 0.61 were observed. The reason for the lanthanide deficiency is not known, but at the relatively low growth temperatures used in ALD (180−350 °C), it is unlikely to be due to thermal decomposition of the precursor. It is more likely that the lanthanide deficiency is intrinsic to the deposition process itself, and detailed mechanistic studies would be required fully to elucidate this. In the $NdAlO_x$ films grown by MOCVD, the Nd/Al ratio shows a marked variation with deposition temperature. The $NdAlO_x$ films grown at 300 and 450 °C are closest to the target 1:1:3 stoichiometry of $NdAlO_3$. The films grown between these two temperatures are neodymium-rich, whereas the films grown at substrate temperatures over 450 °C are aluminum rich. The composition data are similar to those seen previously with $LaAlO_x$ films grown by MOCVD.[11] The trends seen may be due to thermal decomposition of the precursor in the gas phase, leading to partial separation of the Nd and Al components and predeposition of involatile Nd-oxide.

The $PrAlO_x$ films grown by MOCVD do not follow such a pattern. All films grown below 500 °C are praseodymium rich, with an almost consistent Pr/Al ratio of 2:1. This is most likely due to the presence of both the Pr^{3+} and Pr^{4+} oxidation states in the deposited materials, as Pr^{3+} is readily oxidized to Pr^{4+}.

To reduce leakage currents and inhibit the formation of a low-*k* interfacial layer during CMOS processing, it is desirable for the dielectric film to remain amorphous up to relatively high temperature. To investigate this, we annealed samples of $PrAlO_x$ and $NdAlO_x$ films grown by MOCVD at 500 and 400°, respectively, in air over the temperature range 700−900 °C. The X-ray diffraction data of the as-grown samples (see data for $NdAlO_x$ in Figure 6) exhibit only a broad background feature devoid of any crystalline diffraction features (except for a peak at 33° arising from the (200) reflection from the Si(100) substrate). Even after subsequent annealing at 900 °C, both films showed an amorphous structure. Scanning electron microscopy (SEM) was also carried out on the $PrAlO_x$ and $NdAlO_x$ films. The as-grown films showed a featureless morphology. The $PrAlO_x$ retained a featureless morphology after annealing at 900 °C in air for 15 min, but on annealing under the same conditions the $NdAlO_x$ film developed a uniformly spotted microstructure with a feature size of ∼0.1 μm (see Figure 7). Energy-dispersive X-ray analysis of these features showed no significant change in composition from the as-grown $NdAlO_x$

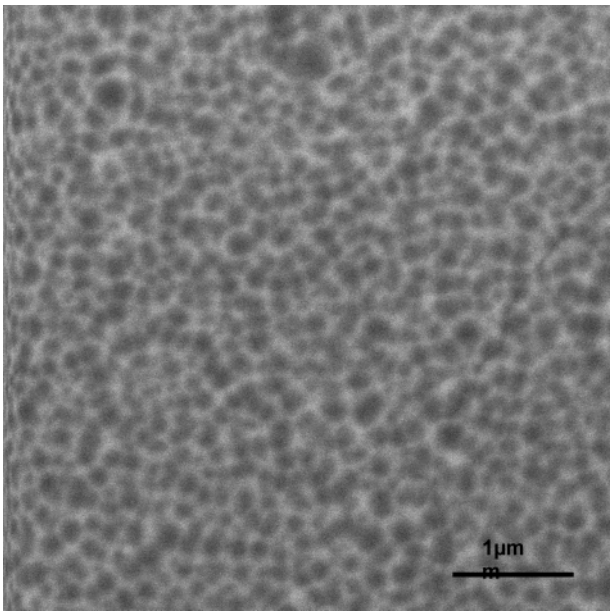

Figure 7. Scanning electron micrograph of a $NdAlO_x$ film annealed at 900 °C in air for 15 min.

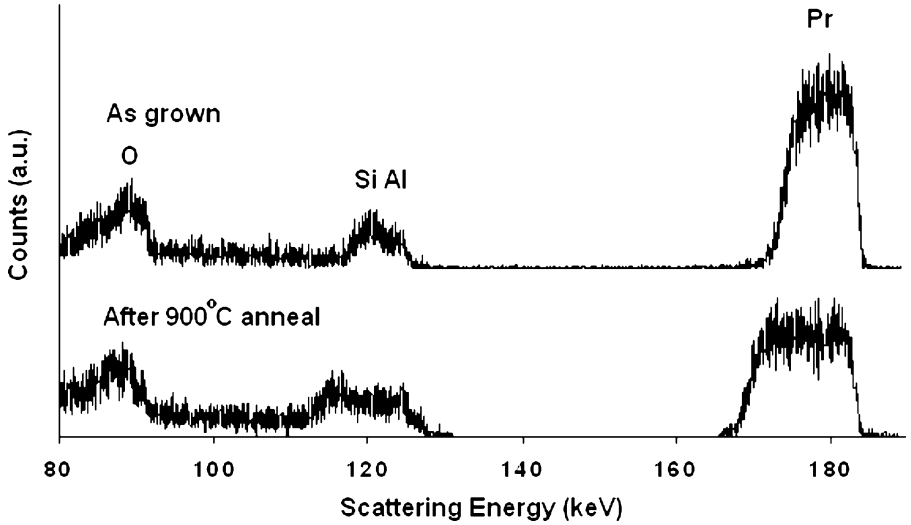

Figure 8. Medium energy ion scattering spectrum of a $PrAlO_x$ film as grown at 350 °C and after annealing at 900 °C in dry air for 15 min.

film. However all ALD films showed no micromorphology when observed in the SEM. This is due to the thin nature of the films.

Medium energy ion scattering (MEIS) has been used to investigate the effect of annealing on the composition and crystallinity of samples of the $PrAlO_x$ and $NdAlO_x$ films. Ion scattering experiments were carried out using the Daresbury MEIS facility. A 200 keV He^+ ion beam was employed with a current of up to 200 nA and a dose per data set of 10 μC. The angle and energy of the scattered ions were determined using a toroidal electrostatic energy analyzer with position-sensitive detector. This allows the simultaneous collection of ions from a 24° range of scattering angles and with a range of energies equal to 2% of the pass energy. The samples were aligned to the ion beam along the [100] channeling direction of the silicon substrate and the electrostatic energy analyzer was positioned to record data along the [111] blocking direction.

The mass of the rare earth element (Pr or Nd) within each of the films is sufficiently greater than the other constituent elements to enable only the rare earth elemental depth distribution to be profiled without interference using the scattering geometry described above. Figure 8 shows the scattered ion energy distribution from a $PrAlO_x$ film deposited by ALD at 350 °C. The scattered He^+ ions undergo inelastic scattering processes as a function of depth below the sample surface. Consequently, the energy distribution gives an effective depth profile of the target atoms. In this case, a depth profile of the rare earth atoms is obtained that indicates the effective thickness of the rare earth aluminate thin film. The thickness of the as-deposited layer in Figure 6 is estimated to be 7 nm. After annealing at 900 °C for 15 min in dry air the praseodymium distribution reduces in intensity but broadens in thickness. This is indicative of some interdiffusion with the silicon substrate, and the same trend is evident from the broadened aluminum distribution that occurs at lower scattering energies. Any crystallization of the layer would usually be accompanied by the formation of an intense surface blocking feature because of registration of the Pr atoms within an ordered phase. No evidence of this is seen, even after annealing at above 1000 °C, which

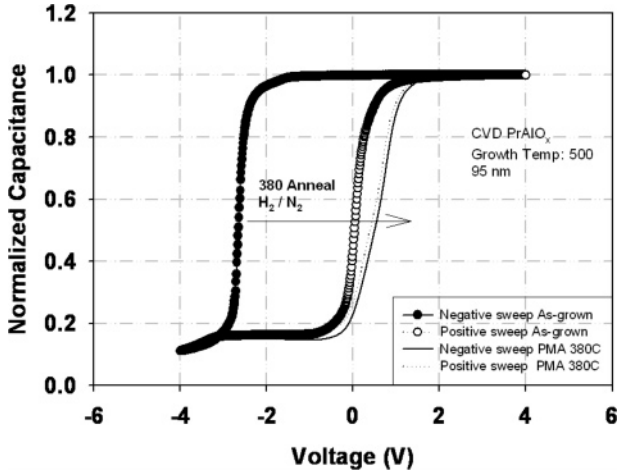

Figure 9. Normalized HFCV curves at 1 MHz for $PrAlO_x$ films (thickness 95 nm) deposited by liquid injection MOCVD before and after PMA in forming gas.

is consistent with the X-ray diffraction observations described above. The resistance of the $PrAlO_x$ films to crystallization is anticipated because of the relatively high content of glassy forming elements such as aluminum and silicon after annealing. The effect of incorporating these elements within the dielectric layer are clearly to suppress the electrical permittivity, which is discussed below. Similar trends were observed for the $NdAlO_x$ thin films; however, annealing above 900 °C was accompanied by loss of rare earth atom intensity, which can only be interpreted by evaporation of a volatile neodymium species from the film surface within the annealing furnace.

To investigate the dielectric behavior of the $PrAlO_x$ films, we tested Al/$PrAlO_x$/n-type Si(100) MOS capacitor (MOSC) structures. Figure 9 shows a comparison of as-grown and post-metalization annealed (PMA) capacitance−voltage ($C-V$) characteristics of the MOSCs. The samples were deposited by liquid injection MOCVD at 500 °C, with a Pr/Al ratio of 0.76, yielding a physical thickness of 95 nm. The $C-V$ curves prior to PMA exhibited a significant hysteresis (~2.66 V) in an anticlockwise direction, indicating significant positive charge trapping. Despite this, the $C-V$ curves did show a steep transition from accumulation to inversion,

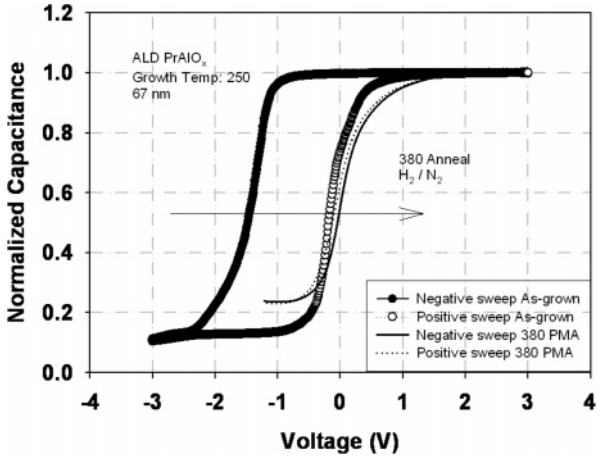

Figure 10. Normalized HFCV curves at 1 MHz for $PrAlO_x$ films (thickness 67 nm) deposited by liquid injection ALD before and after PMA in forming gas.

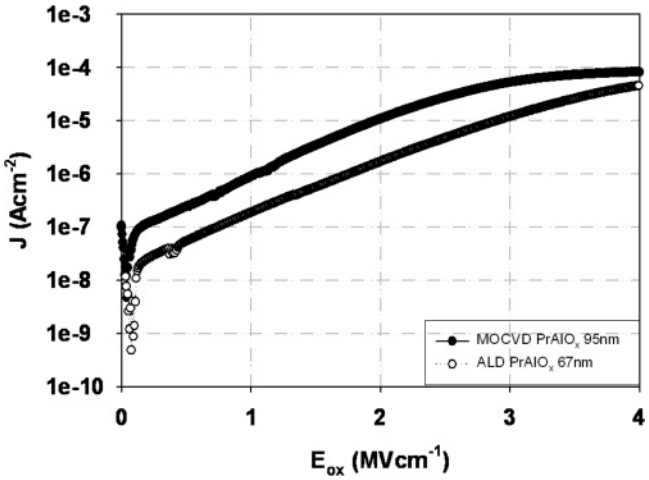

Figure 11. Current density versus electric field for the $PrAlO_x$ films.

indicative of a low interface state density. After PMA, the hysteresis was reduced to a low level (~0.04 V), but interface states may have been created as evidenced by a stretch out of the $C-V$ curves. The relative permittivity calculated from the accumulation capacitance was ~12, assuming a 1 nm interlayer. In Figure 10, normalized $C-V$ curves for the liquid injected ALD $PrAlO_x$ films with a Pr/Al ratio of 0.71 are shown. A significant anticlockwise hysteresis (~1.30 V) was again observed in the as-grown sample. The relative permittivity obtained from the accumulation capacitance was ~14 (assuming a 1 nm interlayer). After a subsequent PMA in forming gas, the resulting capacitance data of these films indicated a reduction in dielectric constant to ~7. The reduction in the measured capacitance and hysteresis after PMA may be due to a removal of some trapped hydroxyls $(OH)^-$ in the dielectrics, which are reported to cause increases in the dielectric constant at lower frequencies and can act as potential trapping sites.[17] The as-grown $PrAlO_x$ films responded well to the forming gas treatment. It is evident that both films also react in a similar manner, thereby reducing the hysteresis to a negligible level. The fixed oxide trap charge density (N_{ot}), assumed to be located near the oxide-semiconductor interface, can be evaluated considering that $N_{ot} = (C_{acc} \times \Delta V_{FB})/(qA)$, where C_{acc} is the accumulation oxide capacitance, ΔV_{FB} is the hysteresis width taken from

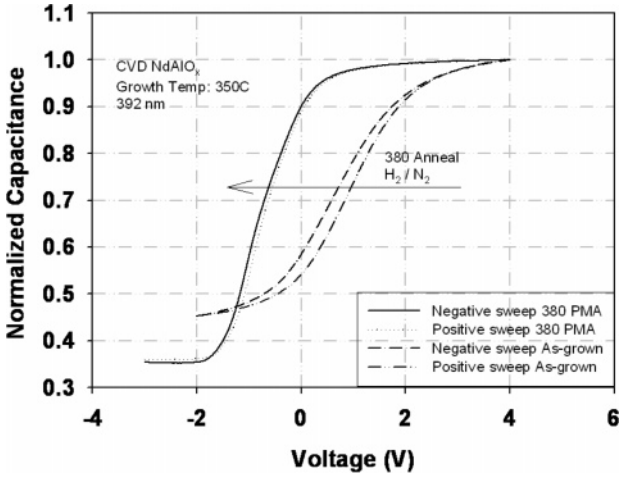

Figure 12. Normalized HFCV curves at 1 MHz for $NdAlO_x$ films (thickness 392 nm) deposited by liquid injection MOCVD before and after PMA in forming gas.

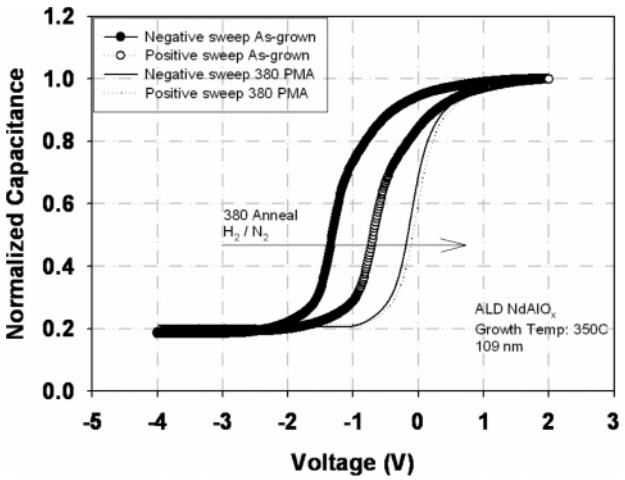

Figure 13. Normalized HFCV curves at 1 MHz for $NdAlO_x$ films (thickness 109 nm) deposited by liquid injection ALD before and after PMA in forming gas.

the extracted flatband voltage of both sweeps, q is the electron charge, and A is the effective electrode area. The positive oxide trapped charge in the as-grown samples (density of 1×10^{12} cm^{-2}) was reduced in both cases to negative 4×10^{10} cm^{-2}; the current−voltage characteristics of both as-grown films are depicted in Figure 11. The current density at 1 mV cm^{-1} was 1×10^{-6} A cm^{-2} for the MOCVD film dropping to 2×10^{-7} A cm^{-2} for the ALD film. These values were an order of magnitude higher than previous studies[17] but are comparable with other high-κ dielectrics (e.g., Pr-silicates,[22] $LaAlO_x$,[11] HfAlO,[23,26] and HfO_2[10,24]).

Normalized high-frequency $C-V$ characteristics for $NdAlO_x$, deposited by MOCVD with an Nd/Al ratio of 0.87, were

(22) Lupina, G.; Schroeder, T.; Dabrowski, J.; Ch, W.; Mane, A. U.; Mussig, H. J.; Hoffmann, P.; Schmeisser, D. *J. Appl. Phys.* **2006**, *99*, 114109.
(23) Kim, S.-H.; Rhee, S.-W. *Chem. Vap. Deposition* **2006**, *12*, 125.
(24) Niinistö, J.; Putkonen, M.; Niinistö, L.; Stoll, S. L.; Kukli, K.; Sajavaara, T.; Ritala, M.; Leskelä, M. *J. Mater. Chem.* **2005**, *15*, 2271.
(25) Van Elshocht, S.; Lehnen, P.; Seitzinger, B.; Abrutis, A.; Adelmann, C.; Brijs, B.; Caymax, M.; Conard, T.; De Gendt, S.; Franquet, A.; Lohe, C.; Lukosius, M.; Moussa, A.; Richard, O.; Williams, P.; Witters, T.; Zimmerman, T. P.; Heyns, M. *J. Electrochem. Soc.* **2006**, *153*, F219.
(26) Lu, Y.; Buiu, O.; Hall, S.; Hurley, K. P. *Microelectron. Reliab.* **2005**, *45*, 965.

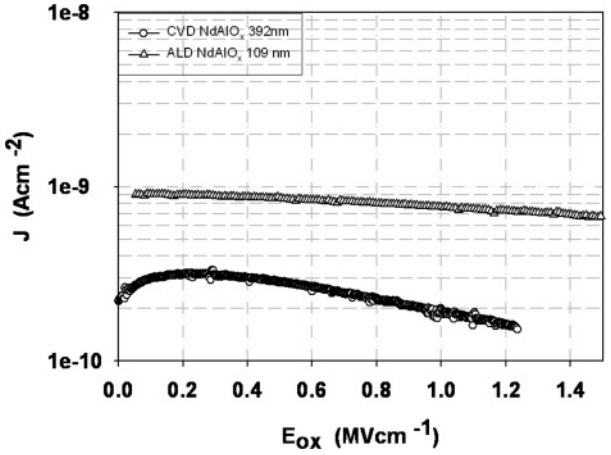

Figure 14. Current density versus electric field for the $NdAlO_x$ films.

depicted in Figure 12. Prior to PMA, the measured $C-V$ curves possessed a small hysteresis (~0.15 V) in the counterclockwise direction. However, the film possessed large interface states evidenced by stretch out of the $C-V$ curves. The relative permittivity prior to PMA was ~14 (assuming a 1 nm interlayer). After PMA, $\kappa \sim 16$ and the oxide trapped charge associated with the hysteresis voltage was below 1×10^{10} cm^{-2}. Figure 13 shows the normalized high-frequency $C-V$ characteristics of $NdAlO_x$ film (thickness 109 nm) deposited by liquid injection ALD with a Nd/Al ratio of 0.42, before and after annealing treatment. Excellent electrical characteristics were obtained after annealing treatment, as seen by the low hysteresis, near-ideal flatband voltage (−0.58V), and a low interface state density. A positively directed flatband voltage shift was observed in this figure, which corresponds to a reduction of fixed positive charges in the oxide layer. Therefore, the PMA reduces both fixed positive charges and oxide trapped charges (density below 1×10^{10} cm^{-2}) for these films according to the time and temperature treatment followed. The relative permittivity calculated from the accumulation capacitance was ~7 (assuming a 1 nm interlayer). This is lower than the permittivity of the $NdAlO_x$ film grown by MOCVD and reflects the higher content of Al_2O_3 ($\kappa \approx 9$) relative to Nd_2O_3 ($\kappa \approx 12.6$) in this ALD film (see Table 4). Current−voltage ($J-E_{ox}$) results (Figure 14) showed that the leakage current density at 1 mV cm^{-1} was 7.5×10^{-10} A cm^{-2} for the ALD-grown film and dropped to 2×10^{-10} A cm^{-2} for the MOCVD-grown film. These leakage currents are more than 1 order of magnitude lower than those obtained for the $PrAlO_x$ (above) and other high-κ previously reported,[10,11] including a recent study on dysprosium scandate.[25] The reduction in current density with increasing electric field for $E_{ox} > 0.3$ mV cm^{-1} is indicative of some electron trapping in the MOCVD-grown films and remains to be investigated further.

Conclusions

Praseodymium aluminate ($PrAlO_x$) and neodymium aluminate ($NdAlO_x$) thin films have been deposited by liquid injection MOCVD over the temperature range 250−600 °C and by liquid injection ALD over the temperature range 180−300 °C. The films were high purity with no carbon detected by AES (est. detection limit ≈ 0.5 at %). The $PrAlO_x$ and $NdAlO_x$ films remained amorphous during annealing up to 900 °C; however, medium energy ion scattering data indicates that the $PrAlO_x$ and $NdAlO_x$ films interact at 900 °C with the Si substrate. The dielectric properties of the $NdAlO_x$ films were superior to those of $PrAlO_x$. $C-V$ and $I-V$ data showed that post-metalized films of $NdAlO_x$ had a permittivity (κ) of ~14 and leakage current densities below 7.5×10^{-10} A cm^{-2}, whereas the $PrAlO_x$ films had a κ value of ~12 with a leakage current density of 1×10^{-6} A cm^{-2}.

Acknowledgment. We thank Epichem Ltd. and the Engineering & Physical Sciences Research Council (EPSRC) for financial support. We also thank Dr. Hywel Davies (Epichem Ltd.) for the TGA data, Dr. Gary Critchlow (ISST, Loughborough University, U.K.) for AES data, and Dr. P. Bailey and Dr. T. C. Q. Noakes for their support for the MEIS experiments made at CLRC Daresbury Laboratory.

CM0707556